model, 0.5 ml/kg of $CCl_4$ is administered twice weekly to C57BL/6 female mice to induce liver cirrhosis, and then GFP-positive BMCs obtained from GFP-Tg mice (C57BL6/Tg14 (act-EGFP) OsbY01 mice)[16] are transplanted through the caudal vein (donor and recipient mice are of the same strain). In this model, we transplanted $1 \times 10^5$ GFP-positive BMCs that had not been cultured. By analyzing GFP-positive BMCs in the recipient mice, we evaluated the repopulation and differentiation of BMCs under conditions of continuous liver injury. Immunostaining, using anti-GFP antibodies,[17] showed that GFP-positive BMCs migrated into the marginal area of hepatic lobules, starting 1 day after BMC transplantation; with time, the distribution of GFP-positive BMCs expanded,[15,18] with they formed a hepatic cord towards the central vein. The use of Liv2, a hepatoblast-specific antibody that we developed,[19] also showed that BMCs first trans-differentiated into Liv2-positive hepatoblasts and then differentiated into albumin-positive hepatocytes. Furthermore, the level of serum albumin significantly increased with time in the recipient mice. These findings suggest that the GFP/$CCl_4$ model can be used to understand the process of BMC differentiation into hepatocytes. On the other hand, GFP-positive cells were not detected in the liver tissues of control mice (those with no liver damage) following BMC transplantation. The persistent liver damage induced by $CCl_4$ injection is important for producing a specific differentiation "niche" in order to activate the plasticity of BMCs and their subsequent differentiation into hepatocytes. Oval cells were thought to be one type of hepatic stem cells derived from the Canal of Hering following severe liver damage.[20,21] Based on the finding of Petersen et al.,[22] that, under some conditions, oval cells are derived from bone marrow cells, we also analyzed the activation of oval cells, using a specific oval-cell marker, A6 antibody. A6-Positive cells were detected in the periportal region 1 week after BMC transplantation in the GFP/$CCl_4$ model, but these A6-positive oval cells did not increase in the 4 weeks after BMC transplantation in this model. We could not detect A6-positive cells that also expressed GFP in the liver after BMC transplantation. These results suggest that, while some signals that activate oval cells are induced by BMC transplantation into $CCl_4$-induced cirrhotic liver, the oval cells may not be derived from transplanted BMCs. In summary, BMCs transplanted into the GFP/$CCl_4$ model trans-differentiated into hepatoblast phenotypes and differentiated into albumin-producing hepatocytes in the "differentiation niche" created by the persistent cirrhosis induced by $CCl_4$ injection.

## Characteristics of candidate BMCs for cell therapy of liver disease

Although various theories explain the existence of pluripotent stem cells in BMCs, the exact composition of the stem cells in BMCs is not clear at present. The following cell types are known to exist in bone marrow: hematopoietic stem cells (HSCs),[13,23] side population cells (SPCs),[24] and mesenchymal stem cells (MSCs).[25] Although past studies used existing antibodies and techniques, there have not been any studies based on the findings of natural liver development studies. The liver functions as a metabolic organ, with the exception of a short period during the fetal stage from embryonic day (E) 12 to 16 (E12–E16), when the liver functions as a hematopoietic organ.[26] We decided to analyze the usefulness of various cell populations of BMCs, based on the analysis of fetal liver development. We prepared a new monoclonal antibody, anti-Liv8 antibody, which recognizes hematopoietic cells using a specific cell-surface marker, in order to identify and separate subpopulations of BMCs capable of differentiating into hepatocytes under $CCl_4$-induced continuous liver damage in the GFP/$CCl_4$ model.[15] Next, we investigated Liv8-positive cells in the BMCs of adult GFP Tg mice. Liv8-positive cells were present in bone marrow in adult GFP-Tg mice; around 32% of BMCs were Liv8-positive. With regard to the relationship between Liv8 and CD45, we found, by flow cytometry, that CD45-positive cells expressed Liv8. These results show that anti-Liv8 is a useful antibody for separating hematopoietic and non-hematopoietic cells. Liv8-positive cells are thought to be hematopoietic cells and Liv8-negative cells are thought to be non-hematopoietic cells. The separated cells were then transplanted into a $CCl_4$-induced liver damage recipient model. At 4 weeks after BMC transplantation, more efficient repopulation and trans-differentiation of BMCs into hepatocytes was seen with Liv8-negative cells. These findings suggest that the subpopulation of Liv8-negative cells includes cells useful for performing cell therapy in damaged livers.[18]

## Improvements in liver function and survival rate, and amelioration of liver fibrosis by BMC transplantation

Using the GFP/$CCl_4$ model, we also evaluated the recovery of liver function and the effect on liver fibrosis and survival rate. Transplanted BMCs trans-differentiated into albumin-producing hepatocytes, leading to an increase in the serum albumin level. Interestingly, we found an amelioration of liver fibrosis after BMC transplantation.[27] Although the exact mechanism of the fibrolysis remains unclear, transplanted BMCs migrated along fibers that had strong expression of matrix metalloproteinase (MMP)-9, resulting in the resolu-

tion of fibrosis. The degradation of the extracellular matrix presumably led to improved liver function, resulting in the better survival of mice following BMC transplantation. We also analyzed differences in liver fibrosis following the transplantation of Liv8-positive or Liv8-negative BMCs. Our results showed that Liv8-negative BMC transplantation ameliorated liver fibrosis to a greater extent than Liv8-positive BMC transplantation. These results show that subpopulations of Liv-8-negative cells will be useful for treating liver cirrhosis. We think that BMC transplantation into liver cirrhosis mice has two effects: BMC trans-differentiation into albumin-producing hepatocytes and the recovery of liver fibrosis.[18,27] These effects of BMC transplantation accelerate the improvement of liver function and the survival rate.

## Molecular mechanisms that regulate the trans-differentiation of BMCs into hepatocytes in the GFP/CCl4 model (microarray-self-organizing map [SOM] analysis)

Recently, cell fusion has been reported to be an important mechanism for the trans-differentiation of BMCs and tissue stem cells.[11,12] The differentiation of BMCs into hepatocytes in the fumarylacetoacetate hydrolase (FAH) model was thought to show the importance of cell fusion in the differentiation of HSCs into hepatocytes.[28,29] However, other groups have reported little evidence of in vivo cell fusion during the trans-differentiation of BMCs into other cell lineages.[14,30] We analyzed the cell fusion rate, using cultured Neo-resistant Embryonic stem (ES) cells and GFP-positive BMCs under the same culture conditions as those used by Terada et al.[11] (cell fusion rate of $1/10^5$–$10^6$), and found similar cell fusion rates in our in vitro assay (data not shown). Mouse hepatocytes have ploidy values of 2N, 4N, 8N, or 16N. The cell fusion of diploid (2N) BMCs with hepatocytes produces cells with ploidy values of 4N, 6N, 10N, or 18N.[28,29] We were afraid that the variety in ploidy values would make it very difficult to analyze cell fusion. We analyzed the DNA ploidy patterns of primary hepatocytes isolated from mice with livers with persistent $CCl_4$ damage, with and without BMC transplantation, at 4 weeks. We were able to isolate around $1.2 \times 10^8$ hepatocytes from recipient mice at 4 weeks by a two-step collagenase method, and we analyzed DNA ploidy patterns by fluorescence activated cell sorting (FACS), We found 2N, 4N, 8N, and 16N DNA bands. Comparisons of these DNA ploidy patterns showed that the 2N and 4N bands were similar, but the peaks, representing 8N and 16N bands, were slightly different (data not shown). These results show that cell fusion may have occurred in the GFP/$CCl_4$ model. Next, we analyzed the differentiation of transplanted BMCs into hepatocytes. Although we could not neglect the possibility that cell fusion had occurred in our model, the BMCs trans-differentiated into Liv2-positive hepatoblasts and functional hepatocytes. We think that the trans-differentiation of BMCs actually occurred in the GFP/$CCl_4$ model. We analyzed the mechanism of this plasticity using DNA chips, which are recently developed tools of genetic analysis. While it is possible to obtain vast amounts of genetic data with DNA chips,[31] interpretation of the factors involved in gene expression requires the application of a statistical technique such as the SOM to visualize the vast amounts of complicated and multidimensional data.[32] In this analysis, we made a specific equation to identify genes that regulate the trans-differentation of BMCs into hepatocytes. In the GFP/$CCl_4$ model, genes related to morphology were dramatically activated at an early stage, while genes associated with hepatocyte differentiation were upregulated at a later state. In the early stage after BMC transplantation, we found that genes such as *FGF* and c-*kit*, as well as *HOX* and *HLH* transcription factors, might be important. In later stages, genes associated with metabolic function, such as hepatocyte nuclear factor 4 (*HNF4*) and glucose-6-phosphatase (*G6Pase*) isomerase were induced, suggesting that, at 4 weeks after BMC transplantation, the transplanted BMCs had begun to assume some of the metabolic functions of hepatocytes.[33] Although many details remain unconfirmed, we think that the microarray-SOM analysis for the GFP/$CCl_4$ model confirms the idea that the BMCs trans-differentiated into immature cells and then differentiated into mature hepatocytes. This information will be useful for understanding the mechanism of BMC plasticity in the GFP/$CCl_4$ model.

## Summary of the lessons learned from the GFP/$CCl_4$ model, and brief report of a clinical study of autologous BMC transplantation into patients with liver cirrhosis

We summarized the findings from the GFP/$CCl_4$ model. As shown in Fig. 1, transplanted GFP-positive BMCs (especially the Liv8-negative cell population, without culturing) migrated into the periportal regions of the cirrhotic liver. With time, the transplanted GFP-positive BMCs trans-differentiated into Liv2-positve hepatoblasts and then differentiated into albumin-producing hepatocytes. The transplanted BMCs formed a hepatic cord. The differentiation "niche" created by the persistent liver damage caused by continuous $CCl_4$ injection is a key factor. Microarry-SOM analysis showed that, at an early stage after BMC transplanta-

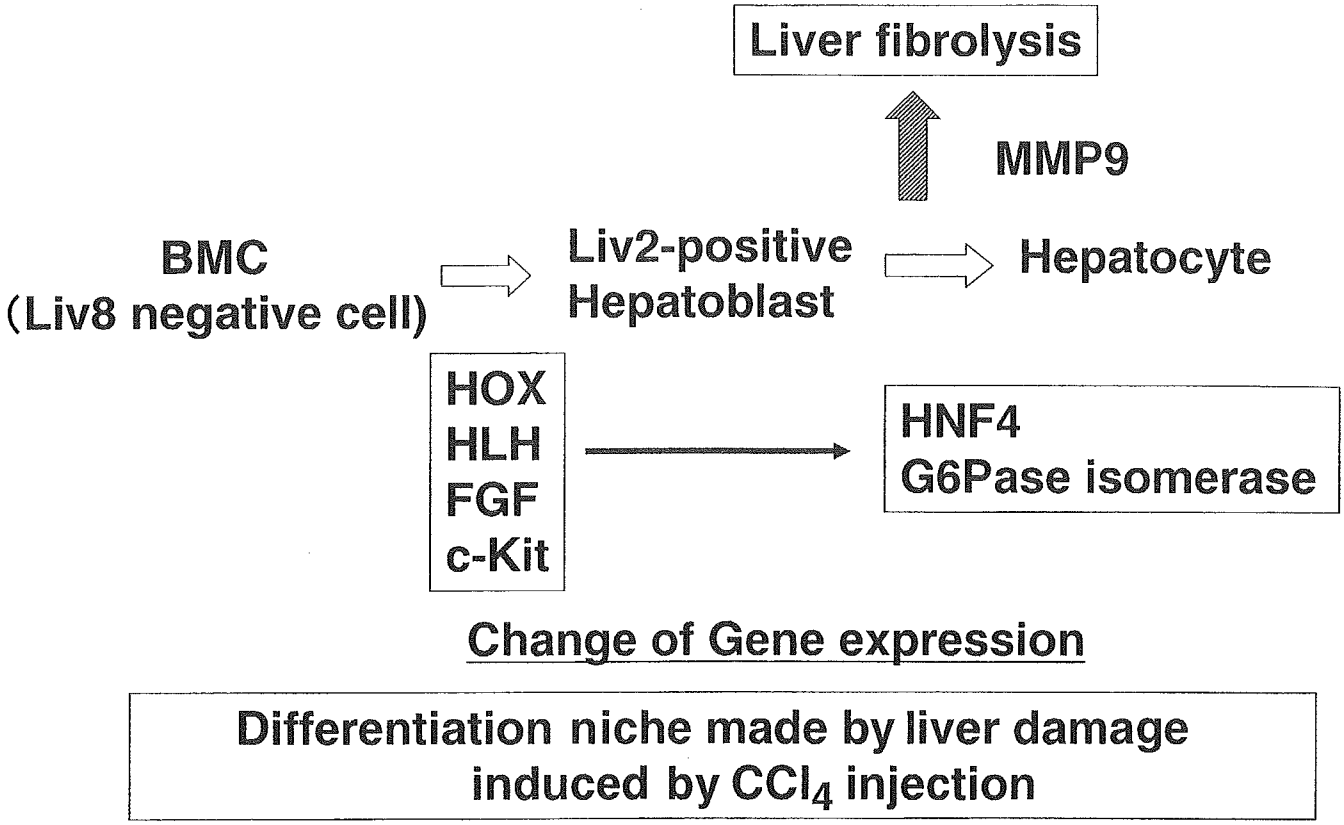


**Fig. 1.** Summary of the green fluorescent protein/carbon tetrachloride (*GFP/$CCl_4$*) model. *BMC*, bone marrow cell; *MMP-9*, matrix metalloproteinase-9; *G6Pase*, glucose-6-phosphatase; *HNF4*, hepatocyte nuclear factor 4

tion, the genes related to morphology were activated, and later, genes associated with liver metabolism were activated. Finally, BMC transplantation improved liver function, ameliorated liver fibrosis, and improved the survival rate. These findings strongly support the development of a new cell therapy, using BMCs, to cure liver cirrhosis, especially because autologous BMC transplantation has few ethical problems and BMC transplantation itself is already an established treatment for hematological diseases. Based on the results obtained in basic research using the GFP/$CCl_4$ model, we prepared a clinical study. We started a phase I clinical study called "Autologous BMC transplantation for liver cirrhosis patients", on November 14, 2003. The study is a first and important step toward the development of a new cell therapy to cure liver failure. We will report the outcome of the phase I clinical study at a later time, and we will combine the basic and clinical studies as part of our translational research, in order to develop a new therapy to cure liver cirrhosis.

*Acknowledgments.* This study was supported by Grants-in-Aid for Scientific Research from the Japan Society for the Promotion of Science (Nos. 13470121, 13770262, 15790348, 16390211, and 16590597) and by a Grant for Translational Research from the Ministry of Health, Labor and Welfare (H-trans-5) of Japan.

## References

1. Alison MR, Poulsom R, Jeffery R, Dhillon AP, Quaglia A, Jacob J, Novelli M (2000) Hepatocytes from non-hepatic adult stem cells. Nature 406:257
2. Theise ND, Nimmakayalu M, Gardnre R, Illei PB, Morgan G, Teperman L, Henegariu O (2000) Liver from bone marrow in humans. Hepatology 32:11–16
3. Korbling M, Katz RL, Khanna A, Ruifrok AC, Rondon G, Albitar M, Champlin RE (2002) Hepatocytes and epithelial cells of donor origin in recipients of peripheral-blood stem cells. N Engl J Med 346:738–746
4. Okamoto R, Yajima T, Yamazaki M, Kanai T, Mukai M, Okamoto S, Ikeda Y (2002) Damaged epithelia regenerated by bone marrow-derived cells in the human gastrointestinal tract. Nat Med 8:1011–1017
5. Terai S, Yamamoto N, Omori K, Sakaida I, Okita K (2002) A new cell therapy using bone marrow cells to repair damaged liver. J Gastroenterol 37(Suppl XIV):162–163
6. Orlic D, Kajstura J, Chimenti S, Jakoniuk I, Anderson SM, Li B, Pickel J (2001) Bone marrow cells regenerate infarcted myocardium. Nature 410:701–705

7. Stamm C, Westphal B, Kleine HD, Petzsch M, Kittner C, Klinge H, Schumichen C (2003) Autologous bone-marrow stem-cell transplantation for myocardial regeneration. Lancet 361:45–46
8. Wexler SA, Donaldson C, Denning-Kendall P, Rice C, Bradley B, Hows JM (2003) Adult bone marrow is a rich source of human mesenchymal "stem" cells but umbilical cord and mobilized adult blood are not. Br J Haematol 121:368–374
9. Hamano K, Li TS, Kobayashi T, Hirata K, Yano M, Kohno M, Matsuzaki M (2002) Therapeutic angiogenesis induced by local autologous bone marrow cell implantation. Ann thorac Surg 73:1210–1215
10. Tateishi-Yuyama E, Matsubara H, Murohara T, Ikeda U, Shintani S, Masaki H, Amano K (2002) Therapeutic angiogenesis for patients with limb ischaemia by autologous transplantation of bone-marrow cells: a pilot study and a randomised controlled trial. Lancent 360:427–435
11. Terada N, Hamazaki T, Oka M, Hoki M, Mastalerz DM, Nakano Y, Meyer EM (2002) Bone marrow cells adopt the phenotype of other cells by spontaneous cell fusion. Nature 416:542–545
12. Ying QL, Nichols J, Evans EP, Smith AG (2002) Changing potency by spontaneous fusion. Nature 416:545–548
13. Krause DS, Theise ND, Collector MI, Henegariu O, Hwang S, Gardner R, Neutzel S (2001) Multi-organ, multi-lineage engraftment by a single bone marrow-derived stem cell. Cell 105:369–377
14. Ianus A, Holz GG, Theise ND, Hussain MA (2003) In vivo derivation of glucose-competent pancreatic endocrine cells from bone marrow without evidence of cell fusion. J Clin Invest 111:843–850
15. Terai S, Sakaida I, Yamamoto N, Omori K, Watanabe T, Ohata S, Katada T (2003) An in vivo model for monitoring transdifferentiation of bone marrow cells into functional hepatocytes. J Biochem Tokyo 134:551–558
16. Okabe M, Ikawa M, Kominami K, Nakanishi T, Nishimune Y (1997) "Green mice" as a source of ubiquitous green cells. FEBS Lett 407:313–319
17. Shinoda K, Mori S, Ohtsuki T, Osawa Y (1992) An aromatase-associated cytoplasmic inclusion, the "stigmoid body," in the rat brain: I. distribution in the forebrain. J Comp Neurol 322:360–376
18. Yamamoto N, Terai S, Ohata S, Watanabe T, Omori K, Shinoda K, Miyamoto K (2004) A subpopulation of bone marrow cells depleted by a novel antibody, anti-Liv8, is useful for cell therapy to repair damaged liver. Biochem Biophys Res Commun 313:1110–1118
19. Watanabe T, Nakagawa K, Ohata S, Kitagawa D, Nishitai G, Seo J, Tanemura S (2002) SEK1/MKK4-Mediated SAPK/JNK signaling participates in embryonic hepatoblast proliferation via a pathway different from NF-kappaB-induced anti-apoptosis Dev Biol 250:332–347
20. Grisham JW, Thorgeirsson SS (1997) Liver stem cells. Academic, Manchester, pp 233–282
21. Petersen BE, Zajac VF, Michalopoulos GK (1998) Hepatic oval cell activation in response to injury following chemically induced periportal or pericentral damage in rates. Hepatology 27:1030–1038
22. Petersen BE, Bowen WC, Patrene KD, Mars WM, Sullivan AK, Murase N, Boggs SS (1999) Bone marrow as a potential source of hepatic oval cells. Science 284:1168–1170
23. Lagasse E, Connors H, Al-Dhalimy M, Reitsma M, Dohse M, Osborne L, Wang X (2000) Purified hematopoietic stem cells can differentiate into hepatocyes in vivo. Nat Med 6:1229–1234
24. Uchida N, Fujisaki T, Eaves AC, Eaves CJ (2001) Transplantable hematopoietic stem cells in human fetal liver have a CD34(+) side population (SP) phenotype. J Clin Invest 108:1071–1077
25. Pittenger MF, Mackay AM, Beck SC, Jaiswal RK, Douglas R, Mosca JD, Moorman MA (1999) Multilineage potential of adult human mesenchymal stem cells. Science 284:143–147
26. Kinoshita T, Miyajima A (2002) Cytokine regulation of liver development. Biochim Biophys Acta 1592;303–312
27. Sakaida I, Terai S, Yamamoto N, Aoyama K, Ishikawa T, Nishina H, Okita K (2004) Transplantation of bone marrow cells reduces $CCl_4$-induced liver fibrosis in mice. Hepatology 40:1304–1311
28. Wang X, Willenbring H, Akkari Y, Torimaru Y, Foster M, Al-Dhalimy M, Lagasse E (2003) Cell fusion is the principal source of bone-marrow-derived hepatocytes. Nature 422:897–901
29. Vassilopoulos G, Wang PR, Russell DW (2003) Transplanted bone marrow regenerates liver by cell fusion. Nature 422:901–904
30. Tran SD, Pillemer SR, Dutra A, Barrett AJ, Brownstein MJ, Key S, Pak E (2003) Differentiation of human bone marrow-derived cells into buccal epithelial cells in vivo: a molecular analytical study. Lancet 361:1084–1088
31. Schena M, Shalon D, Davis RW, Brown PO (1995) Quantitative monitoring of gene expression patterns with a complementary DNA microarray. Science 270:467–470
32. Xiao L, Wang K, Teng Y, Zhang J (2003) Component plane presentation integrated self-organizing map for microarray data analysis. FEBS Lett 538:117–124
33. Omori K, Terai S, Ishikawa T, Aoyama K, Sakaida I, Nishina H (2004) Molecular signature associated with plasticity of bone marrow cells under prsistent liver damage by self-organizing-map-based gene expression. FEBS Lett 578:10–20

for the small GTPase Rab5, is implicated in endosomal dynamics. *Hum. Mol. Genet.* **12,** 1671–1687.

Saito, K., Murai, J., Kajiho, H., Kontani, K., Kurosu, H., and Katada, T. (2002). A novel binding protein composed of homophilic tetramer exhibits unique properties for the small GTPase Rab5. *J. Biol. Chem.* **277,** 3412–3418.

Schmidt, A., and Hall, A. (2002). Guanine nucleotide exchange factors for Rho GTPases: Turning on the switch. *Genes Dev.* **16,** 1587–1609.

Tall, G. G., Barbieri, M. A., Stahl, P. D., and Horazdovsky, B. F. (2001). Ras-activated endocytosis is mediated by the Rab5 guanine nucleotide exchange activity of RIN1. *Dev. Cell* **1,** 73–82.

Topp, J. D., Gray, N. W., Gerard, R. D., and Horazdovsky, B. F. (2004). Alsin is a Rab5 and Rac1 guanine nucleotide exchange factor. *J. Biol. Chem.* **279,** 24612–24623.

Vojtek, A. B., Hollenberg, S. M., and Cooper, J. A. (1993). Mammalian Ras interacts directly with the serine/threonine kinase Raf. *Cell* **74,** 205–214.

Yang, Y., Hentati, A., Deng, H. X., Dabbagh, O., Sasaki, T., Hirano, M., Hung, W. Y., Ouahchi, K., Yan, J., Azim, A. C., Cole, N., Gascon, G., Yagmour, A., Ben-Hamida, M., Pericak-Vance, M., Hentati, F., and Siddique, T. (2001). The gene encoding alsin, a protein with three guanine-nucleotide exchange factor domains, is mutated in a form of recessive amyotrophic lateral sclerosis. *Nat. Genet.* **29,** 160–165.

# [23] Purification and Analysis of RIN Family-Novel Rab5 GEFs

*By* Kota Saito, Hiroaki Kajiho, Yasuhiro Araki, Hiroshi Kurosu, Kenji Kontani, Hiroshi Nishina, and Toshiaki Katada

## Abstract

The small GTPase Rab5 plays important roles in membrane budding and trafficking in the early endocytic pathways, and the activation of this GTPase is mediated by several guanine nucleotide exchange factors (GEFs) at each of the transport steps. The RIN family has been identified as GEFs for Rab5 and shown to possess unique biochemical properties. The RIN family preferentially interacts with an activated form of Rab5, although it enhances guanine nucleotide exchange reaction. Moreover, biochemical analysis indicates that the RIN family functions as a tetramer. In this chapter, we describe the isolation of the recombinant RIN family via expression in *Spodoptera frugiperda* (Sf9) insect cells and in mammalian cells. In addition, functional analysis is also provided to assess the physiological properties of the RIN family.

METHODS IN ENZYMOLOGY, VOL. 403

0076-6879/05 $35.00
DOI: 10.1016/S0076-6879(05)03023-5

## Introduction

The small GTPase Rab5, which cycles between GTP-bound active and GDP-bound inactive states, is involved not only in the homotypic fusion process of early endosomes but also in the budding of clathrin-coated vesicles from plasma membrane and its transport to early endosomes (Zerial and McBride, 2001). The involvement of Rab5 in the many processes indicates that the activation of Rab5 is tightly coupled with the progression of each transport step. In the inactive state, Rab5 forms a cytoplasmic complex with a regulatory protein, Rab GDP-dissociation inhibitor (RabGDI), which prevents an association with improper cellular compartments. However, Rab5 replaces GDP with GTP through its interactions with the guanine nucleotide exchange factors (GEFs) at the target membranes. Rabex-5 was first identified as a mammalian Rab5-GEF, and it contained the sequence homologous to the yeast vacuolar protein-sorting 9 (Vps9) protein (Horiuchi *et al.*, 1997). Vps9p acts as a GEF for Vps21p, a yeast homologue of Rab5 GTPase (Hama *et al.*, 1999). At present, several proteins containing the Vps9 domain that act as GEFs for Rab5 have been identified and considered to regulate certain transport steps in accordance with their regulation and localization (Horiuchi *et al.*, 1997; Kajiho *et al.*, 2003; Otomo *et al.*, 2003; Saito *et al.*, 2002; Tall *et al.*, 2001; Topp *et al.*, 2004).

We recently identified members of a novel family of Rab5-GEFs, RIN2 and RIN3, which contain an Src homology 2 (SH2) domain, proline-rich region, and Ras-association domain in addition to a Vps9 domain (Kajiho *et al.*, 2003; Saito *et al.*, 2002). Intriguingly, the RIN family preferentially interacts with the activated form of Rab5, although it enhances guanine nucleotide exchange reaction on Rab5. Moreover, the RIN family is composed of a homophilic tetramer and interacts with amphyphysin II, which regulates the early steps of the endocytic pathway. This chapter describes the isolation of the recombinant RIN family via expression in *Spodoptera frugiperda* (Sf9) insect cells and in mammalian cells. In addition, a functional analysis is also provided to assess the physiological properties of the RIN family.

## Methods

### *Purification of the FLAG-RIN Family from Sf9 Cells*

*Construction and Selection of RIN-Containing Baculovirus.* Bac-To-Bac Baculovirus Expression Systems were purchased from Invitrogen. pFastBac HTa vectors were mutagenized to FLAG-tagged vectors with polymerase chain reaction (PCR) using following primers.

Sense: 5′ AGGATGACGACGATAAGGATTACGATATCCCAA-CGACC 3′
Antisense: 5′ TGTAATCCATGGTGGCGGTTTCGGACCGAGA-TCCG 3′

Extended double-stranded DNAs were phosphorylated followed by ligation and subcloning. The products were verified by sequencing and renamed pFastBac FLAGa vector. Full-length cDNAs encoding human RIN2 and RIN3 were cloned in the *Eco*RI and *Sal*I sites of the pFastBac FLAGa vectors. These vectors were transformed into DH10Bac competent *Escherichia coli* cells so that bacmids were generated by transposition in *E. coli* cells. The transformed cells were plated in Luria Agar plates containing 50 μg/ml kanamycin, 7 μg/ml gentamicin, 10 μg/ml tetracycline, 100 μg/ml Bluo-gal, and 40 μg/ml isopropyl-β-D-thiogalactopyanoside (IPTG). White colonies were picked up, and the successful transpositions were verified by PCR. The bacmid DNAs were precipitated with the standard alkali method.

*Expression of the RIN Family in Sf9 Cells.* Sf9 cells were grown in EX-CELL 420 (JRH Biosciences) medium supplemented with 100 IU/ml penicillin and 100 μg/ml streptomycin at 27° in a 500-ml glass bottle with stirring. Sf9 cells (approximately $10^6$ cells) were attached in a 35-mm well plate and transfected with bacmids using CellFECTIN reagents (Invitrogen). After 72 h, virus stocks were harvested by centrifuging at 500×*g* for 5 min. To amplify virus stocks, Sf9 cells attached in plates were infected with virus at a multiplicity of infection of 0.01–0.1 for 48 h. Amplification of virus was done twice to obtain higher-titer virus. To produce FLAG-tagged RIN proteins, Sf9 cells were grown to a density of $5 \times 10^6$ cells/ml in a 500-ml glass bottle with stirring. The cells were infected at a multiplicity of infection of 5–10 and incubated for 120 h. The cells were harvested and washed twice with phosphate-buffered saline (PBS) and frozen in liquid $N_2$ before storage at −80°.

*Purification of the RIN Family from Sf9 Cells.* For purification of FLAG-tagged RIN proteins from Sf9 cells, the cell pellet was resuspended with 25 ml of an extraction buffer consisting of 40 m*M* *N*-2-hydroxyethylpiperazine-*N*′-2-ethanesulfonic acid (HEPES)-NaOH, pH 7.4, 75 m*M* NaCl, 15 m*M* NaF, 1 m*M* $Na_3VO_4$, 10 m*M* $Na_4P_2O_7$, 2 m*M* EDTA, 1 μg/ml leupeptin, and 2 μg/ml aprotinin, and subsequently mixed with 25 ml of the extraction buffer containing 2% (w/v) Nonidet P-40 (NP-40). The cell lysate was rotated for 15 min at 4° and then centrifuged at 108,000×*g* for 30 min with an angle rotor. The supernatants were collected and applied to a Bio-Rad open column loaded with Sepharose CL4B (bed volume: 1 ml, Amersham Biosciences). Fractions flowed

through the column were collected and then incubated with a 500-$\mu$l bed volume of anti-FLAG M2 agarose beads (Sigma). After being rotated for 90 min at 4°, the mixture was applied to the open column. The flow-through fraction was again loaded to the column to ensure the maximum binding of RIN proteins to the column. The column was washed twice with 5 ml of a wash buffer consisting of 40 m*M* Tris–HCl (pH 8.0), 1 m*M* EDTA, 100 m*M* NaCl, and 0.6% (w/v) 3-[(3-cholamidopropyl) dimethylammonio]-1-propanesulfonic acid (CHAPS). The protein-bound beads were suspended in 1 ml of the wash buffer containing 100 $\mu$g/ml FLAG peptide (Sigma) and further incubated for 30 min at 4° with occasional vortexing. The eluted fraction was collected, and the beads were further eluted with 1.5 ml of the elution buffer. To remove the FLAG peptide from eluted fractions, the whole fractions were applied to the PD-10 column (Amersham Biosciences) that had been equilibrated with the wash buffer. The void-volume fractions containing RIN proteins were frozen in liquid $N_2$ and stored at −80°. A half-liter culture of the infected Sf9 cells yields approximately 200–300 $\mu$g of FLAG-tagged RIN proteins (Fig. 1A, top panel).

*Assays for Guanine-Nucleotide Exchange and GDP-Dissociation Reactions*

*Materials.* Prenylated Rab5b was purified from baculovirus-infected Sf9 cells according to the method described by Horiuchi *et al.* (1995, see Fig. 1A, bottom), with slight modification: GDP was added to each buffer at a final concentration of 10 $\mu$*M*. Purified Rab5b (180 n*M*) was suspended in a buffer consisting of 25 m*M* Tris–HCl (pH 8.0), 25 m*M* NaCl, 1 m*M* EDTA, 5 m*M* $MgCl_2$, 0.5 m*M* dithiothreitol (DTT), and 0.6% (w/v) CHAPS.

*GDP-Dissociation Reaction.* The dissociation of [$^3$H]GDP was assayed by measuring the decrease in the radioactivity of [$^3$H]GDP-bound Rab5b trapped on the nitrocellulose filters (ADVANTEC). [$^3$H]GDP-bound Rab5b was first made by incubating purified Rab5b (approximately 1 pmol) for 30 min at 30° in a reaction mixture (9.5 $\mu$l) consisting of 20 m*M* Tris–HCl (pH 8.0), 62.5 m*M* NaCl, 10 m*M* EDTA, 5 m*M* $MgCl_2$, 0.5 m*M* DTT, 0.36% (w/v) CHAPS, and 5 $\mu$*M* [$^3$H]GDP (10,000 cpm/pmol). After the incubation, 0.5 $\mu$l of 600 m*M* $MgCl_2$ was added to give a final concentration of 20 m*M*, and the mixture was immediately cooled on ice to prevent the dissociation of [$^3$H]GDP from Rab5b. The dissociation of [$^3$H]GDP from Rab5b was measured in a reaction mixture (65 $\mu$l) consisting of 40 m*M* Tris–HCl (pH 8.0), 62.5 m*M* NaCl, 5 m*M* EDTA, 15 m*M* $MgCl_2$, 0.5 m*M* DTT, 0.36% (w/v) CHAPS, 120 $\mu$*M* unlabeled GDP, and 40 $\mu$*M* GTP in the presence or absence of FLAG-RIN2 and RIN3 (approximately 20 pmol) by incubating at 30° for indicated times. The reaction was stopped

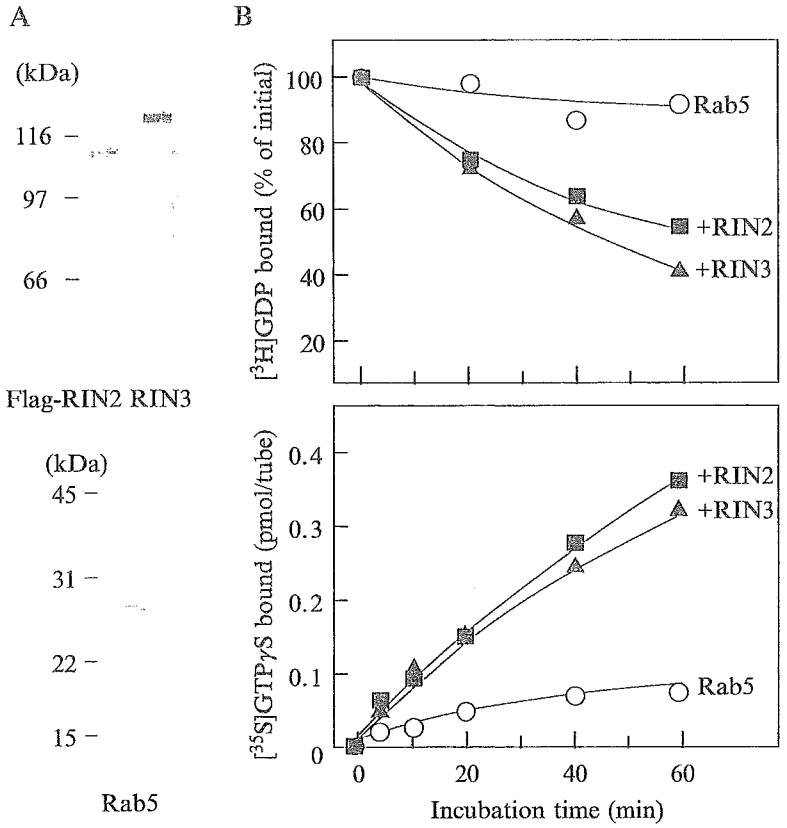


FIG. 1. Analysis of purified RINs and Rab5 by SDS-PAGE and effects of RINs on the guanine-nucleotide exchange reaction of Rab5. (A) Flag-tagged RIN2, RIN3 (top), and prenylated Rab5b (bottom) purified from baculovirus-infected Sf9 cells were separated by SDS-PAGE and stained with Coomassie brilliant blue. (B) Dissociation of [$^3$H]GDP from Rab5b (top) and [$^{35}$S]GTPγS binding to Rab5b (bottom) were measured in the presence or absence of RINs.

by the addition of approximately 2 ml of an ice-cold buffer consisting of 20 m*M* Tris–HCl (pH 8.0), 20 m*M* $MgCl_2$, and 100 m*M* NaCl, followed by rapid filtration on the nitrocellulose filters. The filters were washed five times with the same ice-cold buffer. After filtration, the radioactivity was counted. As shown in Fig. 1B (top), dissociation of [$^3$H]GDP from Rab5b was markedly stimulated in the presence of RIN2 or RIN3.

*Guanine-Nucleotide Binding Reaction.* The binding of [$^{35}$S]GTPγS was assayed by measuring the radioactivity of [$^{35}$S]GTPγS-bound Rab5b trapped on nitrocellulose filters. To avoid nonspecific guanine-nucleotide binding to various proteins, excess amount (50-fold to GTPγS) of ATP was added to the reaction mixture. Purified Rab5b (approximately

1 pmol) was incubated with RIN2 or RIN3 (15 pmol each) in a reaction mixture (50 $\mu$l) consisting of 40 m*M* Tris–HCl (pH 8.0), 62.5 m*M* NaCl, 5 m*M* EDTA, 15 m*M* $MgCl_2$, 0.5 m*M* DTT, 0.36% (w/v) CHAPS, 50 $\mu$*M* ATP, and 1 $\mu$*M* [$^{35}$S]GTP$\gamma$S (20,000 cpm/pmol) at 30° for indicated times. The reaction was stopped by the same method as described for the GDP-dissociation reaction. As shown in Fig. 1B (bottom), [$^{35}$S]GTP$\gamma$S binding to Rab5b was markedly stimulated in the presence of RIN2 or RIN3.

### *Assay for* In Vitro *Association between the Rab5b and RIN Family*

*Preparation of Nucleotide-Bound Forms of Rab5b Proteins.* To prepare GTP$\gamma$S- and GDP-bound forms of Rab5b, the purified protein was incubated with the nucleotides (250 $\mu$*M*) at 30° for 45 min in 11.2 m*M* Tris–HCl (pH 8.0), 50 m*M* HEPES-NaOH (pH 7.5), 110 m*M* NaCl, 0.5 m*M* DTT, 0.27% (w/v) CHAPS, 5 m*M* EDTA, and 2.2 m*M* $MgCl_2$. The reaction was terminated by adding $MgCl_2$ to the final concentration of 10 m*M*.

*Expression of the FLAG-RIN Family in Mammalian Cells.* COS7 or HeLa cells were maintained in Dulbecco's modified Eagle's medium (DMEM) supplemented with 10% fetal calf serum (FCS), 0.16% (w/v) $NaHCO_3$, 0.6 mg/ml L-glutamine, 100 IU/ml penicillin, and 100 $\mu$g/ml streptomycin at 37° in 95% air and 5% $CO_2$. For cell electroporation with FLAG-RIN2 or RIN3, the cells ($1 \times 10^7$ cells) were trypsinized and washed twice with 20 ml of Opti-MEM (Invitrogen) and resuspended in 0.2 ml of Opti-MEM. The cell suspension was mixed with 10 $\mu$g of plasmids and transferred to a 0.4-cm gap cuvette (Bio-Rad) and incubated on ice for 15 min. The cells were resuspended and electroporated at 220 V, 960 $\mu$F with a Bio-Rad Gene Pulser. The cells were diluted with 20 ml of DMEM and cultured for 2 days at 37°.

*Purification of the FLAG-RIN Family from COS7 Cells.* The transfected COS7 cells were washed twice with PBS and solubilized with Buffer A consisting of 40 m*M* HEPES-NaOH (pH 7.4), 75 m*M* NaCl, 15 m*M* NaF, 1 m*M* $Na_3VO_4$, 10 m*M* $Na_4P_2O_7$, 2 m*M* EDTA, 1 $\mu$g/ml leupeptin, 2 $\mu$g/ml aprotinin, and 1% (w/v) NP-40 by vortexing. After gently rotated for 15 min at 4°, lysates were centrifuged at 20,000×*g* for 15 min at 4°. Supernatants were precleared with 20 $\mu$l of anti-mouse IgG agarose beads (50% slurry, American Qualex, Inc.) and immunoprecipitated with 10 $\mu$l of the agarose beads that had been conjugated with 0.5 $\mu$g of the anti-FLAG monoclonal antibody. The beads were washed three times with 1 ml of 20 m*M* Tris–HCl (pH 7.5), 150 m*M* NaCl, and 1% (w/v) NP-40, and three more times with a

buffer consisting of 50 m*M* HEPES-NaOH (pH 7.5), 100 m*M* NaCl, 7.7 m*M* $MgCl_2$, 2 m*M* EDTA, and 0.1% (w/v) NP-40. FLAG-tagged RIN was eluted from the beads with the same buffer containing 1 mg/ml of FLAG peptide.

*Assay for* In Vitro *Association between the Rab5 and RIN Family.* To assay the association between the Rab5 and RIN family, the GDP- or GTP$\gamma$S-bound form of Rab5b was mixed with the anti-mouse IgG agarose beads (10 $\mu$l) containing FLAG-RIN2, FLAG-RIN3, or FLAG peptide alone and incubated at 25° for 60 min in 0.25 ml of 50 m*M* HEPES-NaOH (pH 7.4), 10 m*M* $MgCl_2$, 5 m*M* EDTA, 0.5 m*M* DTT, 100 m*M* NaCl, and 0.1% (w/v) NP-40. The agarose beads were washed four times with a buffer (500 $\mu$l) consisting of 50 m*M* Tris–HCl (pH 8.0), 100 m*M* NaCl, 7 m*M* $MgCl_2$, 2 m*M* EDTA, and 0.2% (w/v) NP-40. Proteins were eluted from the beads with 30 $\mu$l of the same buffer containing 1 mg/ml of FLAG peptide. After centrifugation, 24 $\mu$l of the supernatant was mixed with 8 $\mu$l of 4 × SDS sample buffer, boiled for 5 min, and followed by SDS-PAGE. Immunoblotting was performed with the anti-FLAG M2 monoclonal antibody (Sigma) and the anti-Rab5b polyclonal antibody A-20 (Santa Cruz), respectively.

### *Gel Filtration Analysis of the RIN Family*

*Purification of the Recombinant RIN Family from HeLa cells.* Transfected HeLa cells were washed twice with PBS and solublized with Buffer A then diluted with Buffer A not containing NP-40 to lower the concentration of NP-40 to 0.5% (w/v). After being gently rotated for 15 min at 4°, lysates were centrifuged at 20,000×*g* for 15 min at 4°. Supernatants were precleared with Sepharose CL4B beads (Amersham Biosciences) and immunoprecipitated with anti-FLAG M2 agarose beads by gently rotating for 2 h at 4°. The beads, being washed three times with 0.5 ml of Tris-buffered saline/0.1% (w/v) NP-40, were further washed three more times with Buffer B consisting of 75 m*M* Tris–HCl (pH 7.5), 1 m*M* EDTA, 100 m*M* NaCl, and 0.2% (w/v) NP-40. For SDS-PAGE analysis, the beads were mixed with 24 $\mu$l of Buffer B and 12 $\mu$l of 4× sample buffer and boiled for 2 min. The samples were resolved by SDS-PAGE, and immunoblotting was performed with anti-FLAG antibody.

*Gel Filtration Analysis of the RIN Family.* For gel filtration analysis, the beads were washed six times with 0.5 ml of Buffer C consisting of 25 m*M* Tris–HCl (pH 7.5), 150 m*M* NaCl, and 0.2% (w/v) CHAPS, and subsequently eluted with 0.2 ml of Buffer C containing 1 mg/ml of FLAG peptide by gently vortexing for 1 h at 4°. The eluted fraction was diluted with an

equal volume of Buffer C and applied to a Superdex 200 column (HR 10/30 Amersham Biosciences) that had been equilibrated with Buffer C. Elution was carried out at room temperature at a flow rate of 0.5 ml/min with a fraction volume of 0.25 ml. The fractions were concentrated by precipitation with 10% (final) trichloroacetic acid and subjected to SDS-PAGE and silver staining. The fractions were also analyzed by SDS-PAGE and immunoblotted with anti-FLAG antibody. The elution profile of the column was calibrated with the sizing standards (Oriental Yeast Co. Ltd.) of glutamate dehydrogenase (290 kDa), lactate dehydrogenase (142 kDa), enolase (67 kDa), adenylate kinase (32 kDa), and cytochrome *c* (12.4 kDa).

## References

Hama, H., Tall, G. G., and Horazdovsky, B. F. (1999). Vps9p is a guanine nucleotide exchange factor involved in vesicle-mediated vacuolar protein transport. *J. Biol. Chem.* **274,** 15284–15291.

Horiuchi, H., Ullrich, O., Bucci, C., and Zerial, M. (1995). Purification of posttranslationally modified and unmodified Rab5 protein expressed in Spodoptera frugiperda cells. *Methods Enzymol.* **257,** 9–15.

Horiuchi, H., Lippe, R., McBride, H. M., Rubino, M., Woodman, P., Stenmark, H., Rybin, V., Wilm, M., Ashman, K., Mann, M., and Zerial, M. (1997). A novel Rab5 GDP/GTP exchange factor complexed to Rabaptin-5 links nucleotide exchange to effector recruitment and function. *Cell* **90,** 1149–1159.

Kajiho, H., Saito, K., Tsujita, K., Kontani, K., Araki, Y., Kurosu, H., and Katada, T. (2003). RIN3: A novel Rab5 GEF interacting with amphiphysin II involved in the early endocytic pathway. *J. Cell Sci.* **116,** 4159–4168.

Otomo, A., Hadano, S., Okada, T., Mizumura, H., Kunita, R., Nishijima, H., Showguchi-Miyata, J., Yanagisawa, Y., Kohiki, E., Suga, E., Yasuda, M., Osuga, H., Nishimoto, T., Narumiya, S., and Ikeda, J. E. (2003). ALS2, a novel guanine nucleotide exchange factor for the small GTPase Rab5, is implicated in endosomal dynamics. *Hum. Mol. Genet.* **12,** 1671–1687.

Saito, K., Murai, J., Kajiho, H., Kontani, K., Kurosu, H., and Katada, T. (2002). A novel binding protein composed of homophilic tetramer exhibits unique properties for the small GTPase Rab5. *J. Biol. Chem.* **277,** 3412–3418.

Tall, G. G., Barbieri, M. A., Stahl, P. D., and Horazdovsky, B. F. (2001). Ras-activated endocytosis is mediated by the Rab5 guanine nucleotide exchange activity of RIN1. *Dev. Cell* **1,** 73–82.

Topp, J. D., Gray, N. W., Gerard, R. D., and Horazdovsky, B. F. (2004). Alsin is a Rab5 and Rac1 guanine nucleotide exchange factor. *J. Biol. Chem.* **279,** 24612–24623.

Zerial, M., and McBride, H. (2001). Rab proteins as membrane organizers. *Nat. Rev. Mol. Cell Biol.* **2,** 107–117.

*Human Molecular Genetics, 2005, Vol. 14, No. 6* 1–11
*doi:10.1093/hmg/ddi069*
*Advance Access published on xxx*

# The *Pax6* isoform bearing an alternative spliced exon promotes the development of the neural retinal structure

**Noriyuki Azuma[1,2,*], Keiko Tadokoro[2], Astuko Asaka[2], Masao Yamada[2], Yuki Yamaguchi[3], Hiroshi Handa[3], Satsuki Matsushima[4], Takashi Watanabe[4], Shinichi Kohsaka[5], Yasuyuki Kida[6], Tomoki Shiraishi[6], Toshihiko Ogura[6], Kenji Shimamura[7] and Masato Nakafuku[7]**

[1]Department of Ophthalmology, National Center for Child Health and Development, Tokyo 157-8535, Japan, [2]Department of Genetics, National Research Institute for Child Health and Development, Tokyo 154-8567, Japan, [3]Department of Biological Information, Tokyo Institute of Technology, Graduate School of Bioscience and Biotechnology, Yokohama, 226-8501, Japan, [4]Department of Clinical Pathology, Kyorin University School of Medicine, Tokyo 181-8611, Japan, [5]Department of Neurochemistry, National Institute of Neuroscience, Tokyo, 187-8502, Japan, [6]Department of Developmental Neurobiology, Institute of Development, Aging and Cancer, Sendai 980-8575, Japan and [7]Department of Neuroscience, University of Tokyo Graduate School of Medicine, Tokyo 113-0033, Japan

Received November 28, 2004; Accepted January 18, 2005

**The vertebrate retina has an area where visual cells are closely packed for proper vision that is known as a fovea, an area centralis or a visual streak. The molecular mechanism that regulates the formation of these structures and visual cell gradients is unknown. The transcription factor Pax6 is a master regulator of eye development. A Pax6 isoform that contains an exon 5a-encoded 14 amino acid insertion in its paired domain, Pax6(+5a), has different DNA-binding properties compared with the Pax6(−5a) isoform. Little is known about the functional significance of Pax6(+5a). Here, we show that Pax6(+5a) is expressed especially in the retinal portion where visual cells accumulate during eye development and, when overexpressed, induces a remarkable well-differentiated retina-like structure. Pax6(+5a) proteins that bear point mutations that are found in patients with foveal hypoplasia are unable to induce these ectopic retina-like structures. We propose that Pax6(+5a) induces a developmental cascade in the prospective fovea, area centralis or visual streak region that leads to the formation of a retinal architecture bearing densely packed visual cells.**

## INTRODUCTION

Most vertebrates have a region of the retina where cone photoreceptors, bipolar cells and ganglion cells accumulate and specialize, which contributes to better vision (1–3). This region comes in two general forms, namely, a visual streak and an area centralis. Animals that are nocturnal or have relatively poor vision bear a visual streak, where the photoreceptors, bipolar cells and ganglion cells congregate and become specialized along a horizontal line of the eye fundus. In contrast, animals that have relatively good vision bear the area centralis, which is a circular spot in the retina. The image of an object becomes centered on this region. A specialized form of the area centralis is the fovea, which helps many reptiles and birds, and most primates achieve greater visual sensitivity. The fovea is an area in which cone photoreceptors are highly concentrated and the inner retina is thinned. Human patients lacking the fovea have a poor visual acuity of 0.1–0.3, even with lens correction (4,5). Thus, the fovea is an essential architectural feature that is required for our sharp visual acuity.

In most vertebrates that have a fovea or an area centralis, the retinal cells first accumulate, differentiate and form synaptic connections at the prospective fovea or area centralis

*To whom correspondence should be addressed at: Department of Ophthalmology, National Center for Child Health and Development, 2-10-1 Okura, Setagaya-ku, Tokyo 157-8535, Japan. Tel: +81 334160181; Fax: +81 334162222; Email: azuma-n@ncchd.go.jp

region during the very early stages of eye development, corresponding to the time when ganglion cells appear in the retina. The differentiation of the retinal cells then progresses from the centre to the periphery, which results in a gradient of visual sensitivity (2,3). The molecular mechanisms that regulate the formation of these specific retinal structures are not well elucidated, although previous studies have explored mechanism and genes involved in differentiation of the retinal area (6–8).

Recently, patients with foveal hypoplasia were found to bear mutations in the *PAX6* gene (4,5). The *Pax6* gene encodes a transcription factor and plays important roles in eye morphogenesis in both vertebrates and invertebrates (9–12). This gene has been reported to induce ectopic eye formation in *Drosophila melanogaster* (13) and *Xenopus* larvae (14), and is known as a master control gene in eye formation (9–11). Pax6 is expressed in various eye tissues. In the neural retina, Pax6 is expressed widely in multipotent progenitor cells at early stages and to a lesser extent in ganglion, horizontal and amacrine cells at late stages (15–17). The *Pax6* gene produces two isoforms by alternative splicing, namely, Pax6(−5a) and Pax6(+5a). Pax6(+5a) differs from Pax6(−5a) by the presence of an exon 5a-encoded 14 amino acid insertion in its paired-type DNA-binding domain (paired domain, or PD) (18,19). Pax6(−5a) and Pax6(+5a) show distinct DNA-binding properties (20) and their distinct consensus binding sequences have been determined. These are termed P6CON and 5aCON, respectively (21). Mutational analyses have shown that the N-terminal subdomain (NTS) and the C-terminal subdomain (CTS) of the Pax6 PD are respectively responsible for the DNA-binding abilities of Pax6(−5a) and Pax6(+5a) and their transactivation activity (20,22). Pax6(−5a) binds to a promoter element of the *ζ-crystallin* gene at a site that is highly similar to P6CON (23), while target genes of Pax6(+5a) that bear 5aCON-like sequences are yet to be identified.

Many mutations in the *PAX6* gene have been identified in human patients with foveal hypoplasia (4,5,24–27). In most classical aniridia patients, caused by haploinsufficiency of PAX6 due to its deletion or the presence of a nonsense mutation, all other eye tissues apart from the iris, including the cornea, lens, fovea and optic nerve, are also affected. In contrast, missense mutations in the *PAX6* gene cause more specific eye anomalies (4,5,25–27), probably because Pax6 has multiple functional domains and that missense mutations in this gene disturb one or only a few of these domains. Previously, we reported two PAX6 missense mutations, R128C in the CTS of the PD and V54D in exon 5a, in Japanese patients with foveal hypoplasia (4,5). An R128C mutation was again identified in an independent European patient with the same phenotype (26). These findings suggest that the CTS and exon 5a, which are two elements that are thought to be important for the function of the Pax6(+5a) isoform, may be involved in the formation of the fovea. We investigated expression pattern of Pax6(+5a) in the developing retina and effect of the isoform in retinal development by gain-of-function experiments, and here present evidence that Pax6(+5a) contributes to promote the formation of the retinal structure.

## RESULTS

### Pax6(+5a) is abundantly expressed in the retinal portion where visual cells accumulate

We first examined the regional expression of the Pax6 isoforms by subjecting sections of a neonatal marmoset eye (which has a fovea) to immunohistochemical staining with two different antibodies that can distinguish between the two Pax6 isoforms. One of these antibodies, which is denoted as anti-Pax6, was raised against amino acids 1–223 including those encoded by exon 5a. This antibody reacts with both Pax6(−5a) and Pax6 (+5a), as reported previously (16,17). For this study, we raised another antibody against a synthetic peptide consisting of the 14 amino acid residues that are encoded by exon 5a (anti-exon 5a). Western blotting of proteins prepared from cultured mouse embryonic carcinoma P19 cells that had been transfected with constructs expressing Pax6(−5a) or Pax6(+5a), and of marmoset tissues expressing both isoforms demonstrated the specificity of these antibodies (Fig. 1A). On the marmoset sections, anti-Pax6 visualized three layers, namely, the ganglion cell layer and the inner and outer edges of the inner nuclear layer of the retina. The foveal region was heavily stained, and both the nasal and temporal nasal sides were also stained (Fig. 1C, middle panels). This indicates the wide distribution of Pax6 proteins throughout the entire retina. In contrast, the anti-exon 5a staining pattern suggested that the Pax6(+5a) protein localizes to a restricted retinal area between the optic nerve head and the fovea (Fig. 1C b and c). This was clear when the staining in the nasal and foveal sides of the optic nerve head was compared. The staining was identified scarcely in the nasal side but obviously in the foveal side (Fig. 1C b). From these observations, we conclude that the Pax6(+5a) isoform is expressed especially in the restricted retinal portion where the densely packed visual cells reside.

Reflecting evolutionary conservation of the amino acid sequence encoded by exon 5a, the anti-exon 5a antibody reacts with chicken Pax6(+5a) as well, albeit weakly. In the chicken retina of Hamburger–Hamilton (HH) stage 45, the Pax6(+5a) protein appears to localize in a restricted retinal area of the visual streak, whereas the Pax6(−5a) protein distributes throughout the entire retina (Fig. 2A). To compare the expression levels of the two isoforms, we next performed semi-quantitative RT–PCR analysis using dissected retinal tissues of chick embryos at HH stages 12–45. The isolated RNAs were subjected to RT–PCR analysis using specific primers that flank exon 5a and can distinguish between the two isoforms *Pax6(+5a)* and *Pax6(−5a)*. At an early developmental stage (HH stage12), when the optic vesicle is formed and multipotent progenitor cells still exist in the neural retina, the two isoforms were expressed in both the central nervous system (CNS) and the eye primordium but the *Pax6(−5a)* isoform predominated (Fig. 2B). At HH stage 20, Pax6(−5a) was still the major transcript. At this stage, the formation of the eye is proceeding and lens formation is evident. During HH stages 24–30, the ganglion cells in the retina differentiate. The level of *Pax6(−5a)* expression seems to decrease transiently at HH stage 24 and increase at HH stage 30. Interestingly, the level of *Pax6(+5a)* expression gradually increased during this period

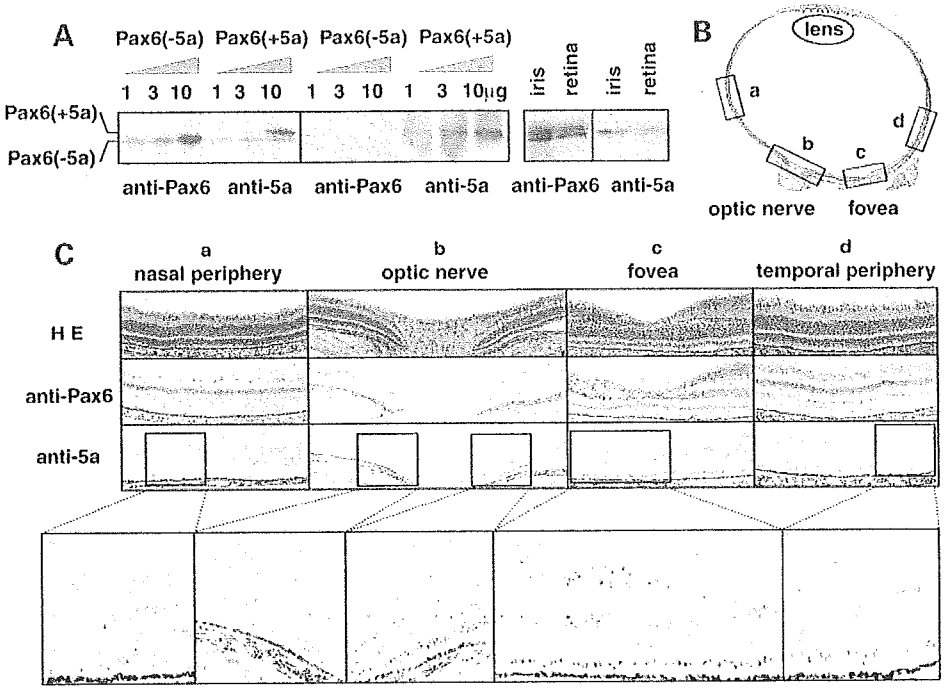


**Figure 1.** Histochemical analysis of the expression of the two Pax6 isoforms in the neonatal marmoset eye. (**A**) Western blotting analysis confirming the specificity of the two antibodies that were used. P19 cells ($10^5$ cells) were transfected with either the Pax6(−5a) or Pax6(+5a) expression construct and nuclear protein fractions obtained 24 h post-transfection were analyzed. Anti-Pax6 recognized the exogenously expressed Pax6(−5a) and Pax6(+5a) proteins as well as endogenous Pax6(−5a) protein, whereas anti-exon 5a recognized Pax6(+5a) but not Pax6(−5a). Western blotting analysis of nuclear fraction proteins obtained from the iris and retina tissues of the neonatal marmoset (*Callithrix jacchus*) also showed that anti-Pax6 recognized both native Pax6(−5a) and Pax6(+5a) proteins, whereas anti-exon 5a recognized Pax6(+5a) but not Pax6(−5a). (**B**) View of a horizontal section of the eye of a neonatal marmoset stained with HE. (**C**) Magnified fields of the eye stained with HE, anti-Pax6 or anti-exon 5a (bar scale 100 μm). Further enlarged images are shown below. a, nasal peripheral area; b, optic nerve head area; c, fovea area; d, temporal peripheral area. The staining for anti-exon 5a localizes around the fovea area, whereas that for anti-Pax6 is detected throughout the entire retina. The result shown is representative of three independent experiments using four marmoset eyes.

in all ocular tissues such as the cornea, lens and retina. Increased expression of *Pax6(+5a)* was also evident in the retina in later stages (HH stages 36–45), when all photoreceptors, horizontal and amacrine cells differentiate. Although the eyes of domestic birds lack the fovea, they possess a distinct visual streak in the posterior portion of the retina (1,2). Expression of *Pax6(+5a)* became particularly intense in this posterior portion. At HH stage 36, the expression of *Pax6(+5a)* exceeded that of *Pax6(−5a)* in the posterior retina. These observations indicate that expression of the two Pax6 isoforms are differentially regulated during retinal development, with Pax6(+5a) expression increasing only in a specified region, whereas Pax6(−5a) expression being throughout the retina.

### In *ovo* misexpression of *Pax6(+5a)* gene markedly expands the retinal layer and promotes the growth and differentiation of retinal cells into visual cells

Next, we investigated the roles the two Pax6 isoforms play in the formation of the eye architecture by *in ovo* electroporation (28). Thus, an expression construct for either Pax6(+5a) or Pax6(−5a) was electroporated into the developing retina of HH stages 16–30 chick embryos, together with an expression construct of green fluorescence protein (GFP) (29) to monitor the expression of the transgenes. Expression plasmids [pCAGGS-PAX6(−5a) and pCAGGS-PAX6(+5a)] carry the entire human *PAX6* coding region with or without exon 5a under the control of a cytomegalovirus enhancer and chicken β-actin promoter, as described previously (5,22). Embryos that had been electroporated were harvested at various stages and analyzed. Retinal formation was scarcely affected when either isoform was transduced after HH stage 30 (data not shown). However, marked changes were observed when either isoform was transduced at HH stages 16–24, when the formation of the optic cup was completed. Six to twelve hours after electroporation of Pax6(−5a) and GFP (HH stage 18), the electroporated region, confirmed by staining with anti-Pax6 and anti-GFP antibodies, was found to proliferate excessively, as evidenced by intense staining with anti-5-bromo-2′-deoxyuridine (BrdU) antibody (Fig. 3). The promotion of retinal cell proliferation occurred similarly up to this stage regardless of the Pax6 isoforms overexpressed (data not shown). Electroporation of the empty vector alone, the pCAGGS-GFP or both constructs did not induce any change.

At later stages, a significant difference in the effect of the two Pax6 isoforms was observed. When Pax6(−5a) was misexpressed, 3–7 days after the electroporation (HH stages 28–35), 47% ($n = 198$) of the eyes were larger than the untreated

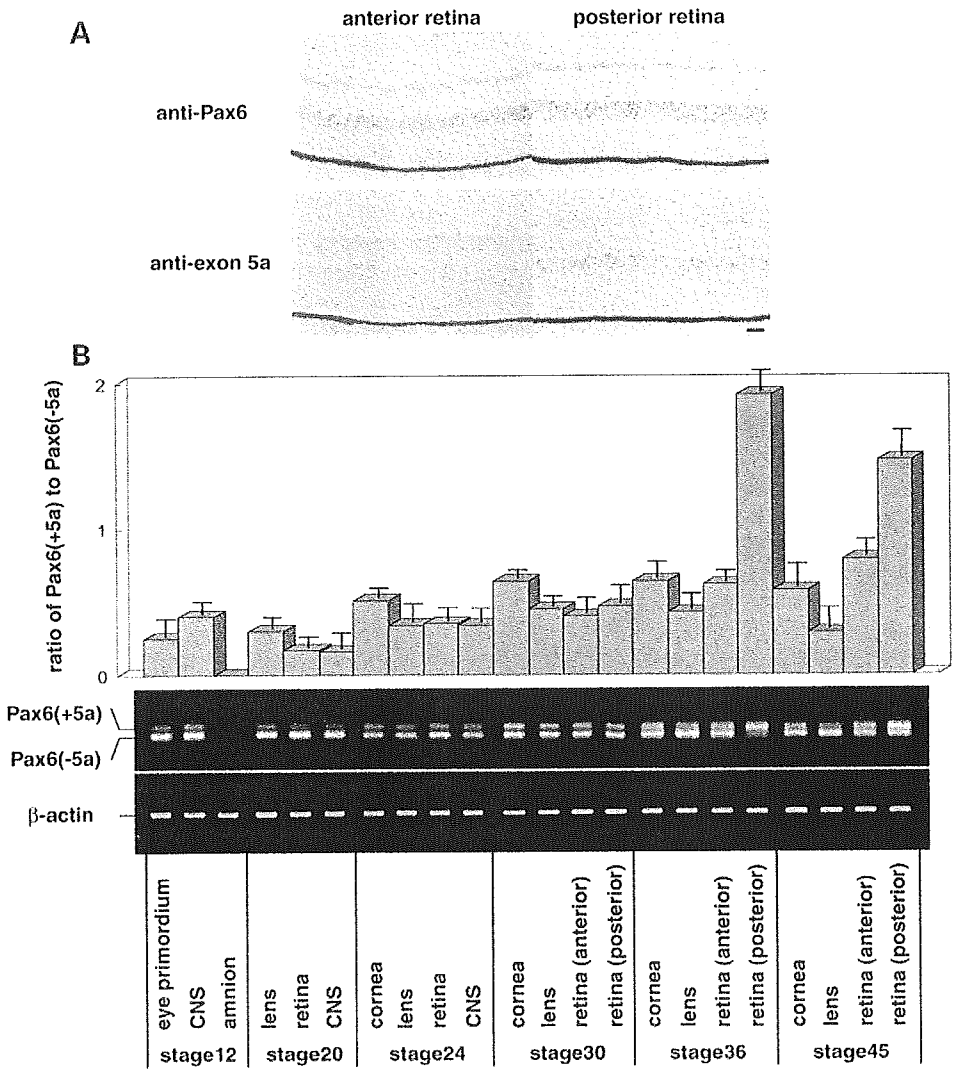


**Figure 2.** (**A**) Horizontal sections of the chick eye at HH stage 45 stained with anti-Pax6 or anti-exon 5a antibody (bar scale 20 μm). The Pax6(+5a) protein appears to localize in the posterior retina containing the visual streak, whereas the Pax6(−5a) protein distributes throughout the entire retina. (**B**) Semi-quantitative RT–PCR analysis of the expression of the two *Pax6* isoforms in developing chick embryos. As the eye became big enough to be dissected at later stages, *Pax6* expression could be examined in particular parts of the eye structure. The indicated PCR fragments were judged to represent one or the other *Pax6* isoform by their sizes. This was confirmed by sequencing. In the posterior retina, tissues were excised from the visual streak region. Amnion tissues were used as a negative control for *Pax6* expression and *β-actin* represents the amounts of RNA in each lane. The bar graph is shown as mean ± SD ($n = 3$) of expression ratio of Pax6(+5a) to Pax6(−5a). The photograph of RT–PCR analysis under the bar graph is representative of three independent experiments.

control eyes (Fig. 4A). Several isolated swelling spots (bulges) or lines (wrinkles) on the retina were observed in 68% of the 198 treated eyes. Green fluorescence was also observed at these areas (Fig. 4B). Histological examination showed that the retina was thickened and staining with anti-Islet1 and anti-neurofilament antibodies revealed that the differentiation of ganglion cells had expanded to the surface layer at these places (Fig. 4C). In 32% ($n = 198$) of the Pax6(−5a)-treated eyes, an embankment-like structure swelled out on the retina. In addition, several fibres (10–100 μm in length) grew out into the vitreous cavity (Fig. 4D). Sections were stained with specific antibodies for Islet1, a homeodomain-containing transcription factor that is expressed in the ganglion cells in the developing retina (30), and neurofilament protein, an intermediate filament protein specific to retinal neurons (31). The immunohistochemistry suggested that the fibres in the vitreous cavity were nerve bundles derived from ganglion cells (Fig. 4E). These abnormal structures may be caused by the unbalanced growth and differentiation of the retina, because the nerve fibres extended onto the retinal surface and formed additional layers on the retina.

When the Pax6(+5a) isoform was misexpressed instead of Pax6(−5a), more dramatic changes were observed inside the enlarged eyes 3–7 days after electroporation (HH stages 28–35). Of the 187 treated eyes, 6% had a wall-like structure protruding into the vitreous cavity, which was shown to be a

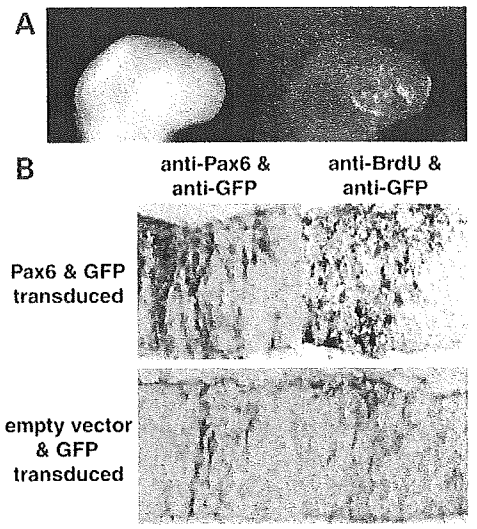


**Figure 3.** Early changes in the developing chick eye induced by the electroporation of Pax6(−5a). Constructs expressing Pax6(−5a) and GFP were electroporated into the right eye primordium of HH stage 16 chick embryos ($n = 5$). (**A**) Twelve hours after electroporation (HH stage 18), expression of GFP in the right eye was examined using fluorescence microscopy. (**B**) Sections double-immunostained with anti-GFP (violet) and anti-Pax6 (brown) and anti-GFP (violet) and anti-BrdU (brown) antibodies show the expression of the electroporated GFP and Pax6(−5a) constructs and the pronounced proliferation of the retinal progenitor cells around the electroporated area, but transduction of empty vector, pCAGGS-GFP or both constructs did not induce any change ($n = 5$ for each). (bar scale 20 μm). Transduction of the Pax6(+5a) isoform had a similar effect on eye development at these stages ($n = 5$; data not shown).

folded retina by histological analysis (Fig. 4G and H) and 42% showed thick stick-like structures protruding from the retina into the vitreous cavity (Fig. 4I and J). These protruding structures were very long and some even approached the lens on the opposite side. Cross sections of these protrusions were subjected to *in situ* hybridization with probes specific for *Musashi*, which encodes a neural RNA-binding protein highly enriched in neural precursor cells (32), *Six3*, a homologue of *Drosophila* homeobox gene *sine oculis*, that is expressed in inner and outer nuclear layers (33), and *Rx*, a paired-class homeobox gene, which is expressed in the inner nuclear layer, presumably bipolar cells of the developing retina (34). Immunohistochemical staining with anti-ISlet1 and anti-neurofilament antibodies was also performed (Fig. 4K). These analyses suggested that the tubular structures consist of well-differentiated retinal layers, which include nerve fibres, ganglion cells and developing inner and outer nuclear layer cells, with an outer surface layer of nerve fibres and an inner surface of photoreceptor cells. These tubular and fold structures suggest that the horizontal overgrowth of the neural retinal layer occurred at the regions where Pax6(+5a) was misexpressed. As space was limited even in the enlarged eyeball, the regional expansion of the cells seemed to push the retinal layer up into the vitreous cavity. Such drastic outgrowths that contain all retinal cell types was never obtained when Pax6(−5a) was misexpressed. Electroporation of the empty vector alone or the pCAGGS-GFP or both constructs did not induce any phenotypic changes. Thus, we conclude that the Pax6(+5a) isoform can induce horizontal overgrowths of the retina that protrude into the vitreous cavity. Of the 187 treated eyes, 34% of the Pax6(+5a)-treated eyes, which showed protrusion of the retina, became significantly larger than untreated control eyes (Fig. 4F). Although we have reproducibly generated this protruding retina by electroporating at HH stages 16–24, such morphological alterations were not induced when the electroporation was performed at later stages. Transduction of Pax6(−5a) or Pax6(+5a) using an adenoviral vector or electroporation using smaller amounts of plasmid DNAs caused similar, although somewhat weak phenotypic changes (data not shown). The incidence of the Pax6(−5a)- and Pax6(+5a)-dependent eye architectural changes at each stage is available in Supplementary Material.

We next examined the distribution of photoreceptor cells in the protruding retinal structures. Embryos were allowed to develop just before hatching (HH stages 40–45) and then analyzed. Some lectins, including peanut agglutinin and wheat germ agglutinin, specifically stain cone photoreceptor cells (35), which are normally condensed at the visual streak in the posterior portion of the chick eye (Fig. 5A and B e region). Histochemical examination revealed that the cone cells were detectable in the folded retina not only near the visual streak (d region) but also in the peripheral portion (c region) where lectin-staining is normally negative as observed in an unaffected peripheral portion (b region). Colour opsins are components of cone cells (2,3,36). RT–PCR showed that three types of colour *opsins* were expressed in the peripheral and posterior portions of the folded retina (c and d regions) at a similar level as in an unaffected region in the posterior portion of the retina (e region), and more intensely than an unaffected region of the peripheral portion of the retina (b region) (Fig. 5D). In contrast, the expression level of *rhodopsin*, a component of rod cells, was high in the peripheral areas and low in the visual streak (2,3). The peripheral portion of the folded retina (c region) exhibited *rhodopsin* expression at a similar level as the control peripheral area, whereas the expression level in the affected region in the posterior portion of the retina (d region) was similar to that in the visual streak (e region). These results suggest that the differentiation of retinal cells is highly promoted in the protruding retina to the level seen in the visual streak with regard to both the layer structure and the density of cone cells.

### Effect of missense mutations of the *Pax6* gene on retinal overgrowth

To understand which element or structure of Pax6 is important for inducing the retinal overgrowth observed, we introduced several mutations into the Pax6 PD: (a) the R26G mutation in the NTS (25), (b) the R128C mutation in the CTS (4) or (c) the V54D mutation in exon 5a (5). The transactivation potentials of wild-type and mutant Pax6 with or without exon 5a have been assayed previously (5,22) or in this study using reporter genes containing P6CON or 5aCON, which are consensus binding sites for the (−5a) and (+5a) isoforms, respectively. As summarized in Figure 6A, the NTS in Pax6(−5a) wild-type is responsible for P6CON-binding,

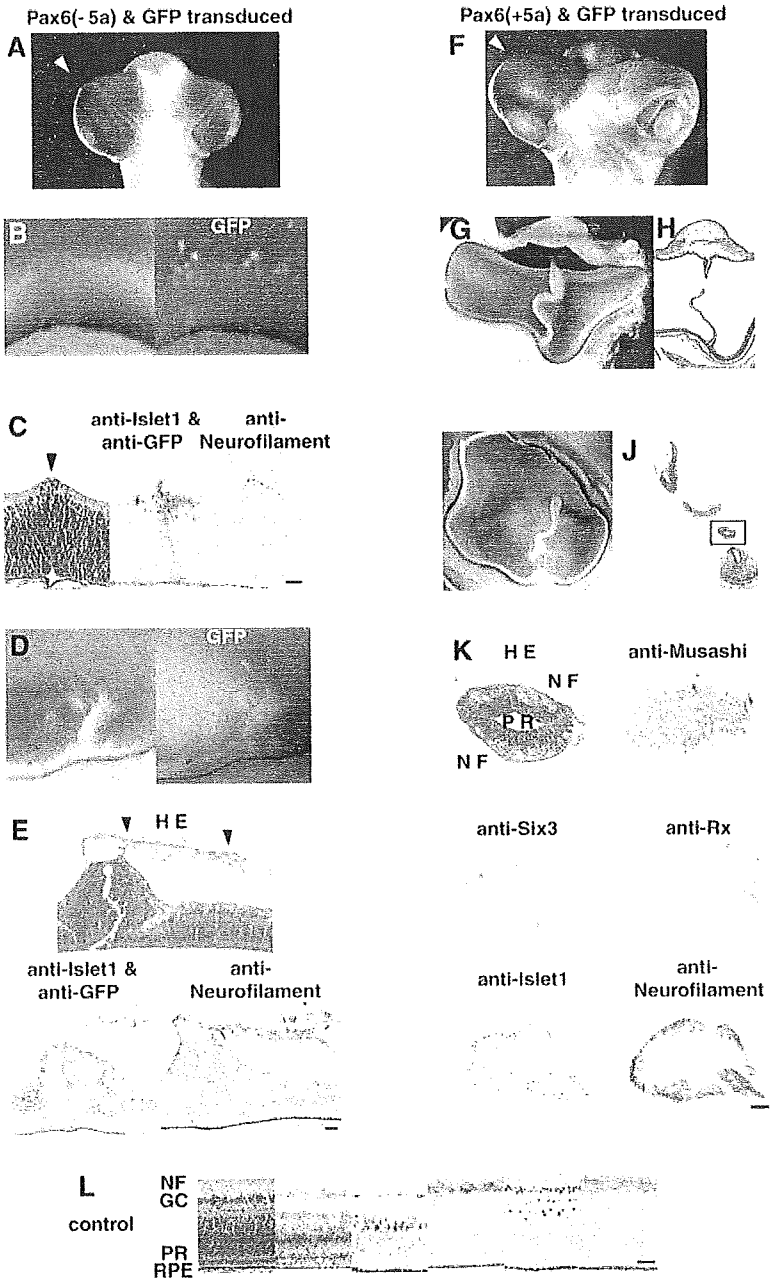


**Figure 4.** Later changes in the developing chick eye induced by electroporation of Pax6(−5a) (**A–E**) or Pax6(+5a) (**F–K**) together with GFP. (A–C) A Pax6(−5a)-transduced embryo at HH stage 30. (A) The frontal view shows an enlarged eye (arrowhead). (B) The inside views show several areas of swelling on the retinal layer with green fluorescence (the right panel, matched field). (C) Sections stained with HE, anti-islet1, anti-GFP and anti-neurofilament antibodies. Islet1 (brown) and GFP (violet) were double-stained. Ganglion cells (arrowhead) excessively differentiated in the surface layer of the thickened retina where the electroporated GFP constructs is expressed (bar scale 20 μm). (D, E) A Pax6(−5a)-transduced embryo at HH stage 34. (D) A view of the split eyeball shows embankment-like swelling from the retina with numerous fibres with green fluorescence (matched field). (E) Numerous fibres grow from the embankment-like retina into the vitreous cavity (arrowheads). Sections immunostained with anti-ISlet1 (brown), anti-GFP (violet in the left lower panel) and anti-neurofilament (brown) antibodies show expression of the electroporated constructs and ectopic growth of the nerve bundles from the retina (bar scale 20 μm). (F–H) A Pax6(+5a)-transduced embryo at HH stage 34. (F) A frontal view shows a significantly enlarged eye that breaks through the eyelid skin (arrowhead). Views of the split eyeball (G) and section with HE staining (H) show that the retina overgrows to show fold structure. (I–K) A Pax6(+5a)-transduced embryo at HH stage 36. Views of the split eyeball (I) and section with HE staining (J) show that the retina overgrows into stick structure. GFP expression was weak and could not be detected in the aberrantly growing tissues. (K) Analysis of the boxed region of the section indicated by (J) by *in situ* hybridization using probes specific for *Musashi, Six3* and *Rx* and immunohistochemistry with anti-islet1 and anti-neurofilament antibodies. These analyses suggest that the aberrantly growing tissues in the Pax6(+5a)-transduced eyes are composed of well-differentiated retina layers (bar scale 20 μm). NF, nerve fibres; PR, photoreceptors. (**L**) A portion of the posterior retina normally developing at a corresponding stage is illustrated for comparison. NF, nerve fibres; PR, photoreceptors; RPE, retinal pigment epithelium (bar scale 20 μm).

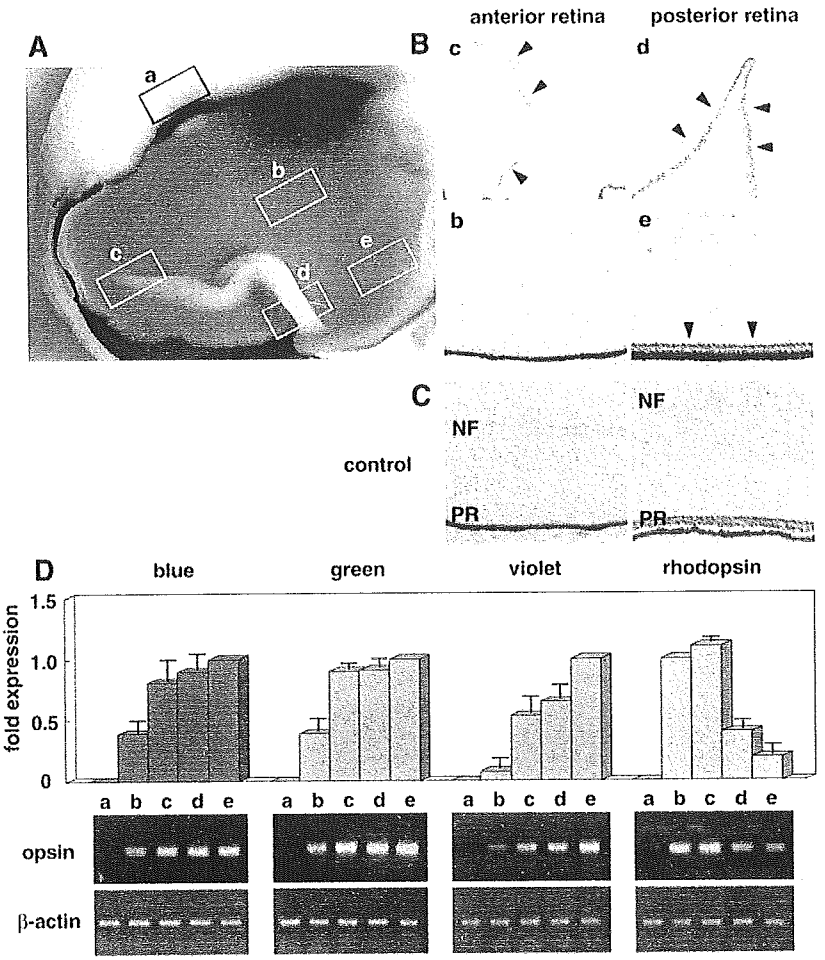


**Figure 5.** Differentiation of photoreceptor cells in the extruding and folded retina induced by electroporation of Pax6(+5a) at HH stage 18. **(A)** A view of a split eyeball at HH stage 45 shows the folded retina. Five areas were examined: (a) the cornea, (b) an unaffected region in the peripheral portion of the retina, (c) a peripheral portion of the folded retina, (d) a posterior portion of the folded retina and (e) an unaffected region in the posterior portion of the retina including the visual streak. **(B)** Staining with peanut agglutinin shows the presence of cone photoreceptor cells in the c region as well as in the d and e regions (arrowheads). **(C)** A portion of the retina normally developing at a corresponding stage is also illustrated for comparison. NF, nerve fibres; PR, photoreceptors (bar scale 20 μm). **(D)** Semi-quantitative RT–PCR demonstrates the expression of three colour *opsins* (*blue, green* and *violet*) and *rhodopsin* in the various regions. The bar graphs are shown as mean ±SD ($n = 3$) of ratio of expression in a–d region to that in e region (blue, green and violet *opsins*), or ratio of expression in a or c–e region to that in b region (*rhodopsin*). The photograph of RT–PCR analysis under the bar graph is representative of three independent experiments using six treated eyes.

while in Pax6(+5a) wild-type, the insertion of 14 amino acids encoded by exon 5a into the NTS abolishes its NTS P6CON-binding activity and unmasks the CTS 5aCON-binding ability. The R26G mutation in the NTS strongly impairs the NTS- and P6CON-mediated transcriptional activation of Pax6(−5a) and increases the CTS- and 5aCON-mediated transcriptional activation of Pax6(+5a). In contrast, the R128C mutation in the CTS abolishes the CTS- and 5aCON-mediated transcriptional activation of Pax6(+5a), and hyperactivates the NTS- and P6CON-mediated transcription activation of Pax6(−5a). The V54D mutation in exon 5a has a weak inhibitory effect on the CTS-and 5aCON-mediated transcriptional activation, but increases the NTS- and P6CON-mediated transcriptional activation. Thus, it has been proposed that the two subdomains negatively regulate each other, and exon 5a thus appears to function as a molecular switch that determines target gene specificity. When these mutants were misexpressed in the primordial retina of HH stages 16–30 chick embryos, only Pax6(+5a) R26G and Pax6(−5a) R128C induced a phenotypic change. Retinal overgrowth was observed in 34% and 26% of the eyes that had received Pax6(+5a) R26G ($n = 54$) and Pax6(−5a) R128C ($n = 56$) respectively, although the observed phenotypic changes were less significant than those induced by the respective wild-type Pax6 isoforms. Morphological changes induced by Pax6(+5a) R26G were more drastic than those induced by Pax6(−5a) R128C. Retinal swelling and string- and stick-like structures induced by Pax6(+5a) R26G (Fig. 6B), and fibres induced by Pax6(−5a) R128C (Fig. 6C) are shown as examples. The incidence of eye architectural changes by transduction of

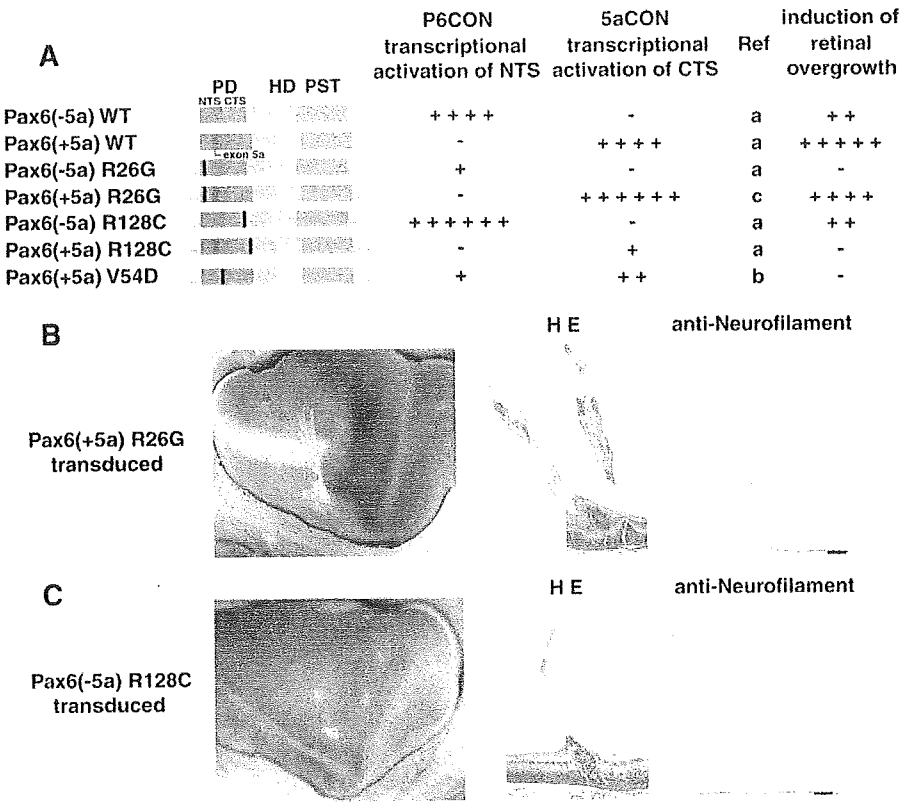


**Figure 6.** Effect of missense mutations of the *Pax6* gene on retinal overgrowth. (**A**) Schematic structure of the Pax6 wild-type and mutant (R26G, R128C and V54D) proteins with or without exon 5a that were used in this study. Our *in vitro* functional assays using P6CON- and 5aCON-CAT reporters in P19 cells have been reported previously [a, Yamaguchi *et al.* (22); b, Azuma *et al.* (5)] or are reported for the first time in this study (c). The effects of the mutants on overgrowth of the retina are also summarized. PD, paired domain (red, NTS; purple, CTS; blue, exon 5a; black bar, missense mutation); HD, homeodomain; PST, proline–serine–threonine rich transactivating domain. Each of the Pax6 mutants was electroporated into the right eye of HH stage 16 chick embryos and the changes around HH stage 35 were observed. (**B**) An eye that misexpresses Pax6(+5a) that carries the R26G mutation. The split eyeball shows the string- or stick-like structure of the overgrowing retina (left panel) (Pe, the pecten). Sections stained with HE and anti-neurofilament antibody suggest that the overgrowing tissues are thick bundles of nerve fibre and immature retina tissues (right panels, bar scale 100 μm). (**C**) An eye that misexpresses Pax6(−5a) that carries the R128C mutation. The split eyeball shows areas of swelling on the retina with fine fibres (left panel). Sections stained with HE and anti-neurofilament antibody reveal excessive differentiation of ganglion cells and their nerve fibres (right panels, bar scale 100 μm).

each mutant at each developmental stage is available in Supplementary Material.

## DISCUSSION

We have shown here that when Pax6 is overexpressed in the developing chick eye, it induces ectopic differentiation of the retina. Compared with the effect of Pax6(−5a), Pax6(+5a) induces a remarkable artificial retina-like structure. Intriguingly, the ectopic retina-like structure induced by Pax6(+5a) is highly differentiated and contains well-formed retinal layers that express cone-specific colour opsins. We believe that the retinal overgrowth reported here is not an artifact but rather an exaggeration of the natural role of Pax6(+5a) in retinal development, namely, in the formation of the retinal area where visual cells highly accumulate. The assumption is based on two lines of evidence, as described subsequently.

First, Pax6(+5a) is expressed in a region of the developing retina where visual cells are densely packed (Figs 1 and 2). Previous studies have revealed that Pax6(+5a) is abundantly expressed in the lens and iris (37,38), but the expression pattern of Pax6(+5a) in the retina has not been clarified. As shown in previous studies and in the study reported here, the expression of the two Pax6 isoforms in the developing eye seems highly regulated at the levels of transcription and mRNA splicing (39,40).

Secondly, there is a clear correlation between the mutations in Pax6(+5a) that are associated with abnormal foveal formation in humans and that affect ectopic retinal formation in chick embryos. The V54D and R128C mutations disturbed the ectopic retinal structures induced by Pax6(+5a) as shown in Figure 6, while previous genetic analyses showed that these mutations are associated with foveal hypoplasia in human patients (4,5,26). As the V54D mutation in exon 5a should not affect the structure of Pax6(−5a), these observations suggest that Pax6(+5a) probably plays an important role in the formation of the fovea. Curiously, the V54D